Edelweiss Applied Science and Technology
ISSN: 2576-8484
Vol. 9, No. 2, 2042-2063
2025
Publisher: Learning Gate
DOI: 10.55214/25768484.v9i2.5043

Preparation and characterization of Li-Zn-Barium ferrite nano powder for bio applications

Saffa'a Hussein Ali[1*], Zena Mohammed Ali Abbas[2]
[1]Department of Physics, College of Science, University of Diyala, Iraq; saffaah9@gmail.com (S.H.A.).
[2]Department of Physics, College of Science, University of Diyala, Iraq; zenaalbana@yahoo.com (Z.M.A.A.).

Abstract: Substituted barium hexaferrite, represented as $BaFe_{12-2x}Li_xZn_xO_{19}$ (where x values are 0.2, 0.4, 0.6, and 0.8), was synthesized using the auto-combustion sol-gel technique. This research examined the structural features and magnetic properties of barium ferrite with varying quantities of non-magnetic replacements (Zn^{2+} and Li^{+} ions) via various analytical methods. The processed XRD powder patterns confirmed the existence of a single-phase structure, indicating that both Zn^{2+} and Li^{+} ions successfully integrated into the barium hexaferrite lattice without disrupting its hexagonal structure. FTIR spectra displayed prominent bands associated with barium hexaferrite and hydroxyl (OH) groups. The EDS results confirmed the successful incorporation of the non-magnetic cations into the structure. FESEM images showed that all samples exhibited a hexagonal phase, and as the substitution of cations in the barium ferrite structure increased, the particle size decreased. Furthermore, with an increasing x value, the grains tended to elongate into rod-like shapes. The saturation magnetization (Ms) and remanent magnetization (Mr) both decreased, reaching minimum values of 5.462 emu/g and 7.08 emu/g, respectively. In contrast, the coercive field (Hc) increased significantly, particularly at x = 0.4, where it reached a maximum value of 4358 Oe. The squareness ratio (Mr/Ms), which exceeded the theoretical value of 0.5, confirmed that the hexaferrite powders demonstrated strong uniaxial anisotropy.

Keywords: *Auto-combustion sol-gel technique, Saturation magnetization and coercivity, Structural and magnetic properties, Substituted barium hexaferrite.*

1. Introduction

Hexaferrites are highly valued for their unique physical properties, making them suitable for a variety of technological applications. For applications involving permanent magnets, a large coercive field is essential. In contrast, magnetic recording technology requires a lower coercive field alongside increased saturation magnetization. Thus, it is crucial to tailor the magnetic properties Cation substitution serves as an effective approach to modifying hexaferrites, allowing them to meet the specific demands of diverse applications. M-type hexagonal ferrites, represented by the formula $MFe_{12}O_{19}$ (where M can be Ba, Sr, or Pb), an elevated Curie temperature, strong coercivity, remarkable chemical stability, pronounced uniaxial magnetic anisotropy, and excellent resistance to corrosion [1]. Magnetic ferrites are prepared as a dense polycrystalline nano powder composed of a highly effective and biologically compatible material that is of great interest in contemporary research. In our hypothesis, we propose that the Li-Zn-Barium nano powder should exhibit even greater specific absorption rate maxima and improved uptake performance compared to traditional materials. These specifically fabricated nano-sized materials find diverse applications across a multitude of fields such as electronics, ceramics, and they hold significant promise for use in various medical investigations and applications. The exceptional magnetic property of these materials is meticulously controlled by the incorporation of different types of transition metals, which play a crucial role in determining their magnetic characteristics. Importantly, these ferrites exhibit a

History: Received: 9 December 2024; Revised: 20 January 2025; Accepted: 20 January 2025; Published: 26 February 2025
* Correspondence: saffaah9@gmail.com

superparamagnetic behavior, which makes them particularly valuable in enhancing cancer therapies, especially when exposed to an alternating magnetic field. The biological applications arising from the use of superparamagnetic ferrites have shown to yield markedly improved results due to the unique properties inherent to these materials when compared to their counterparts. Furthermore, the ferrite materials may also have considerable applicability in thermoluminescence, catalysis, and in efforts to destroy pathogenic bacteria. This application is especially effective at elevated temperatures, where the formation of hydroxyl free radicals can facilitate the degradation of harmful microorganisms, thus underscoring the versatility and effectiveness of these nanomaterials in both medical and industrial contexts.

Furthermore, this research work also investigates the numerous possibilities for effectively utilizing these remarkable characteristics of Li-Zn-Ba nano material. The careful ratios of zinc and ferrite employed in this context could significantly facilitate the latest and most innovative methods in the field .

The floating or implementation of processes such as co-precipitation, catalysis, and microemulsion—especially for the purpose of creating new materials with enhanced properties such as lower system costs or improved solubility—presents a very attractive option for in-depth pharmaceutical studies. This research further explores the intricate methodology and rigorously tests various properties, including crucial structural values and solubility metrics. Subsequently, it was subjected to testing for various biological applications and efficacy in real-world scenarios, yielding promising results in the vitality tests conducted on the bacteria involved .

Looking ahead, additional comprehensive studies will be undertaken to explore testing in either in vitro or in vivo environments, allowing for an expansive and thorough investigation. For a complete study, it would be of considerable interest to utilize nontoxic materials, thereby providing a significant opportunity within the health field. In a general sense, the novel nano materials of ferrite that exhibit good magnetic properties will prove to be indispensable for future studies focused on cancer therapy applications, as well as numerous other uses. These applications stand to benefit from the simple preparation of biocompatible iron oxide materials, wherein it is crucial to avoid the detrimental toxic effects typically associated with iron oxide in bio applications. Recently, barium hexaferrites ($BaFe_{12}O_{19}$, also known as BaM) have attracted considerable interest from researchers for these applications. Studies show that zinc and lithium (Li) Substituted barium hexaferrites are interesting materials for magnetic recording technologies and microwave devices.. The substitution of non-magnetic zinc and lithium ions has been found to increase saturation magnetization while reducing the coercive field. Research on non-magnetic ion-substituted barium hexaferrites has been extensive, with numerous reports on bimetallic alternatives that include zinc and other cations [2]. In this our work , we going to Examine the structural and magnetic characteristics of BaFe12-2xLixZnxO19 hexaferrite powders, where x equals 0.2, 0.4, 0.601, and 0.802. The powders were produced using the sol-gel auto-combustion technique. Our results demonstrate that the replacement of Fe^{3+} ions with Li^{+} and Zn^{2+} ions significantly modifies the structure and magnetic characteristics of the BaFe12-2xLixZnxO19 hexaferrite powders. Furthermore, we evaluated the Anti.Ba. activity of the materials against bacteria, including Staphylococcus aureus and Proteus mirabilis.

2. Literature Review

The existing literature has provided substantial evidence indicating that Li-Zn-Barium ferrite could indeed emerge as an excellent candidate for a wide range of bio applications in the medical and technological fields. It is characterized by a unique and unprecedented mix of properties, prominently featuring both magnetic and electrical properties that allow it to be distinctly set apart from other products that are commonly available on the market [3]. These remarkable device properties are not just arbitrarily assigned attributes; rather, they stem from the intrinsic and fundamental properties of the materials themselves, which renders them not only particularly valuable but also highly appealing for a variety of technological applications and innovations across diverse sectors. Nonetheless, it must be noted that as of now, there exists only a limited number of published papers that meticulously detail this

Edelweiss Applied Science and Technology
ISSN: 2576-8484
Vol. 9, No. 2: 2042-2063, 2025
DOI: 10.55214/25768484.v9i2.5043

fascinating topic, specifically within the actual nano scale range, which remains of primary interest among researchers both from natural settings and industry alike [4]. Ceramics that are known and categorized as ferrites are synthesized through a range of different established methods, including coprecipitation, sol-gel, and sol-combustion processes, all of which come with their own distinct advantages as well as specific conditions that can impact the outcomes. The predominance of the sol-combustion method will underpin the present investigation, standing out among the many synthesis techniques that could be employed [2]. This particular technique has provided consistently optimistic performance, efficiency, and scalability metrics for practical applications, thereby making it an attractive and viable route for future investigations and research endeavors. After conducting an exhaustive and thorough literature search, the interrelated preparation processes, characterization techniques, and diverse studies focused on biofield applications have been defined in a well-organized, cross-linked, and consistent manner to enhance overall understanding. This diligent analysis contributes significantly to providing a clearer and more in-depth understanding of the extraordinary potential and capabilities of Li-Zn-Barium ferrite in various bio-innovations, which could possibly pave the way for groundbreaking advancements and significant breakthroughs in the rapidly evolving field of biomedical technologies and applications. The researchers have been actively exploring an extensive myriad of innovative and fascinating methods to synthesize a wide range of diverse nanomaterials that serve specialized purposes. Generally, the established synthesis methods that are commonly recognized and validated within the scientific community include well-established techniques such as co-precipitation, sol-gel, sol-combustion, as well as various dry methods, each contributing to the rich tapestry of material science [5]. Consequently, in their fervent pursuit of obtaining effective and optimized properties of these cutting-edge materials, researchers have been conducting numerous detailed experiments and meticulously reporting their findings in various interconnected contexts related to these synthesis procedures. However, the summarized results that have been obtained by these dedicated researchers over time often appear to present somewhat contradicting views and inconsistent findings, leading to an ongoing dialogue, debate, and discussion in the field regarding the efficacy and reliability of these methodologies. On the other hand, researchers have also been genuinely striving for advancements in the critical realm of bioengineering to effectively tackle and handle complex issues related to cancer, along with significant tissue engineering applications, particularly through the utilization of ferrites. The primary reason for channeling focused efforts in this direction is that magnetite nanoparticles, especially after being coated with appropriate and suitable magnetic materials, not only possess the remarkable capacity to deliver cancer cells, various types of drugs, and stents directly to the targeted site but they also exhibit a fascinating ability to release drugs thanks to the application of an external magnetic field following the unloading of the drug itself at the specified location. Up until the present time, numerous different types of ferrites, particularly superparamagnetic nano ferrites, have been meticulously developed and rigorously tested, all with the objective of discovering and identifying biocompatible nano ferrites that can be effectively utilized and employed in a variety of medical applications and therapeutic interventions. However, it is noteworthy that the specific composition known as Li-Zn-Barium nano ferrites has yet to be synthesized and characterized in sufficient detail to substantiate their functionalities for a diverse range of relevant bio applications [6]. The reports and the findings available in the existing literature thus far have not adequately discussed the comprehensive nano range associated with such nanoferrites, indicating a gap that needs to be addressed. Furthermore, the dedicated researchers have reported and successfully synthesized aero particulates exceeding 50 nm in size and evaluated only their biological properties; however, they have yet to delve more deeply into thoroughly probing and examining the inherent magnetic properties that are present above the established nano range, indicating a need for further investigation in this crucial area [7].

3. Experimental Work

Prepare the [$BaFe_{12-2x}Li_xZn_xO_{19}$] nanoparticles at 950°C, using varying values of x= 0.2, 0.4, 0.6, and 0.8. The diagram illustrates the materials used in the preparation of the samples, Nanophase materials

Edelweiss Applied Science and Technology
ISSN: 2576-8484
Vol. 9, No. 2: 2042-2063, 2025
DOI: 10.55214/25768484.v9i2.5043

and nano power have recently attracted much attention for their small size and very high surface area. In an extensive set of disciplines spanning bio and medicine, knowledge about physical, chemical and thermal characteristics of nanoscale powders is key. Through a co-precipitation route, we synthesize the Li0.47Zn0.18Ba0.25Fe1.5-yLayO4 nano powder and elucidate its promising merits from biomedical and bio applications. We have conducted a comprehensive chemical analysis to study the system comprising percentage composition, determination of particle size (using x-ray particle size subject analysis), surface morphology (via scanning electron microscopy). The x-ray diffraction technique will have a role in the determination of phase purity, extent of crystallinity, and further elucidation of the crystallographic structure of the samples. The measurable characteristics were also discovered to be influenced by the crystal size, the non-uniform lattices strain, and the appearance of some mineral forms, e.g., the amorphous and the microcrystalline phases, etc. Scanning electron microscopy was employed to further scrutinize the ferrite-polymers' surface features and additional physical properties, such as crystallite shape, conditional structure, etc. According to the source, the range of those materials is broad, and qualitative and quantitative data can be acquired from 20 nm to 20,000 nm. We need to examine the transmission electron microscopy to see whether the structural properties, including things such as lattice structure, impurities, etc., could be detected. Through high-resolution transmission electron microscopy it has been possible to delineate embedded microstructural characteristics in the ferrite polymers. The successful implementation of nanostructured materials in real-world contexts hinges on their performance, which is determined by the architecture and chemical makeup of the materials themselves. The new frontier for nanomaterials is the biological field. Mossbauer spectroscopy is adept at collecting kinetic information on ferrite grains. Those parameters related to structures are found to have a solid dependence on the synthesis method, including particle size, cation distributions, and eventually atomic positions. The X-ray diffraction method is capable of determining crystal structure, phase composition, and crystallinity. High-resolution imaging of spin coating variances documented in terms of roughness by scanning electron microscopy further illustrates the various surface morphology of field-exposed structures along with surface topography. Polycrystals can be regularly characterized at fine detail by transmission electron microscopy now that it has been widely adopted across many fields. After acquiring the selected area diffraction data, we can construct a diffraction pattern representative of the sample. We proceed to characterize the spacing between adjacent planes, obtain the relevant plane indices, and determine the three-dimensional structure of the cubic lattice to be face-centred. For Xu0.48Zn0.18Ba0.26Fe0.95O4 and Xu0.52Zn0.185Ba0.13Fe0.55La0.45O4 compounds, the Langmuir theory estimated average particle sizes ranged from 31 to 41 nm and the best fitting methods (in terms of calculating this D parameter from the obtained XRD peaks) seem to show the same trends for each compound as with the other methodologies as well. This size particle is therefore capable of exhibiting a high level of magnetism. Including the sintered process. This information is presented in Figures 1.

Edelweiss Applied Science and Technology
ISSN: 2576-8484
Vol. 9, No. 2: 2042-2063, 2025
DOI: 10.55214/25768484.v9i2.5043

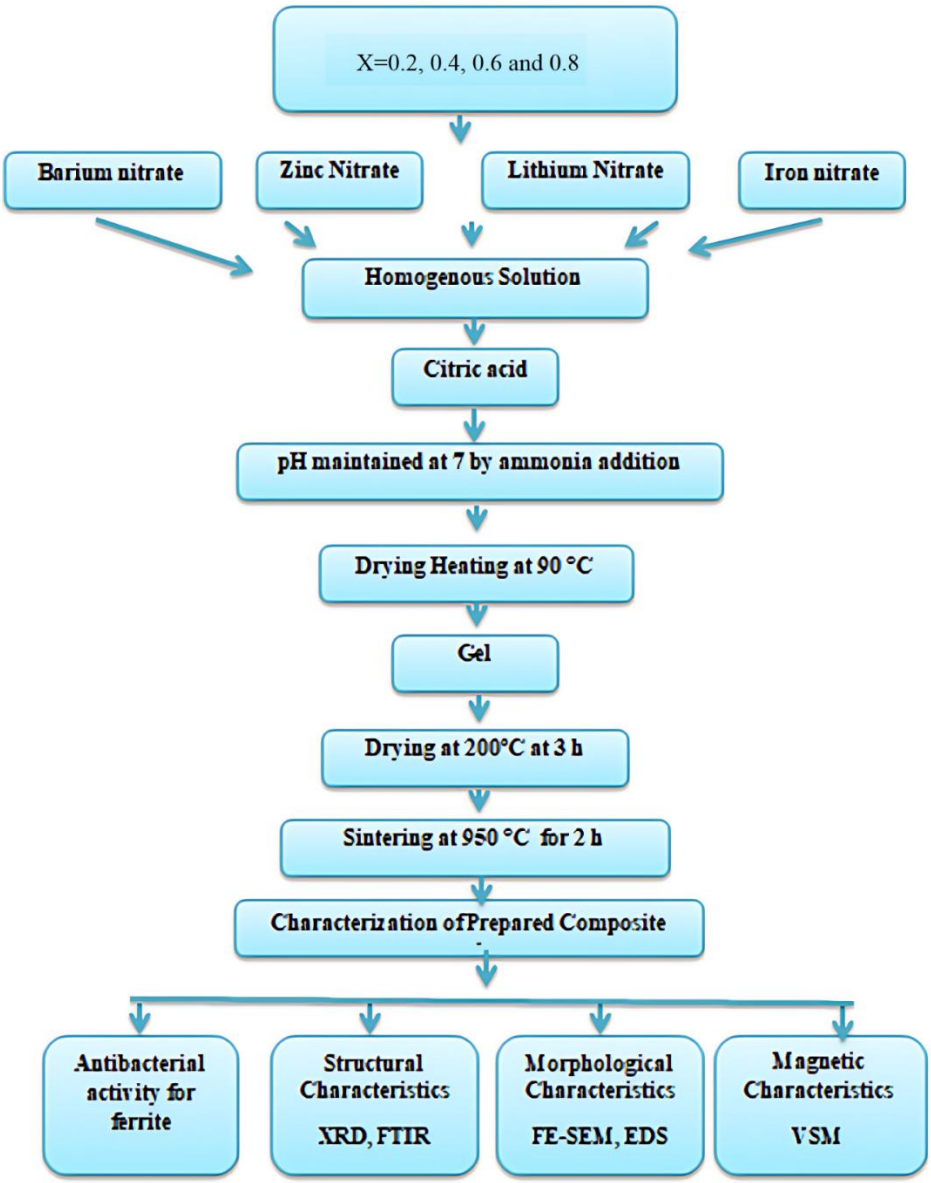

Figure 1.
Flow chart of preparation and characterization of [Ba Fe12-2X Lix ZnxO19] ferrite NPs.

Edelweiss Applied Science and Technology
ISSN: 2576-8484
Vol. 9, No. 2: 2042-2063, 2025
DOI: 10.55214/25768484.v9i2.5043

4. Laboratory Equipment Used

The tools and equipment used in this study to prepare BaFe12O19 nanoparticles include Pyrex beakers (Glassco, UK; BORO 3.3). The raw materials were carefully weighed using a sensitive electronic balance (Nimbus NBL 254e, Adam Equipment, China). A hot plate with a magnetic stirrer (Atur a.LFA, D-500, China) was employed to heat and stir the solution, ensuring the necessary temperature was maintained. A mortar and pestle were used to grind the prepared nan powders. To sinter the samples at different temperatures, an electric furnace from Labtech (Korean) was used, along with silica crucibles. The dimensions of the furnace are 40 x 20 x 20 cm. The FT system was regulated by a programmable control unit, "Eurotherm."." Figure 2 depicts all of the equipment mentioned.

Figure 2.
Equipment used in this investigation.

5. Preparation of Ferrite Materials

5.1.Preparation of [Ba Fe_{12-2x} Li_x Zn_x O_{19}] ferrite, where (x = 0.2, 0.4, 0.6, and 0.8).

Metals nitrate (Iron nitrate, Barium nitrate, Lithium Nitrate, Zinc Nitrate) and citric acid in mole ratio of citric acid : nitrates = 1:1 are dissolved separately in distilled water according to the molar ratios, as shown in figure (3a). The nitrate solution was combined with the acid solution in a Pyrex flask, used a magnetic stirrer to mix with citric acid, while adding drops of ammonia to adjust the pH to around 7. as seen in figure (3b). Combine the components for thirty minutes at ambient temperature. to ensure mix homogeneity. Continue to stir the liquid while increasing the temperature gradually until it reaches 90°C until a highly viscous residue of dried gels is fored, as shown in figure (3c). To breakdown the organic precursor and gaseous volatiles The viscous gel is placed in oven heated to 200°C about 180 minuts and creates as-burnt ferrite, as illustrated in the fig (5.1d). by process of burning, the desiccated gel undergoes a transformation into a finely textured powder exhibiting a dark gray coloration, so indicating the initiation of the production of ferrite with a high degree of purity. as illustrated in the figure (3e).To

Edelweiss Applied Science and Technology
ISSN: 2576-8484
Vol. 9, No. 2: 2042-2063, 2025
DOI: 10.55214/25768484.v9i2.5043

enhance crystallization and achieve a uniform distribution of activity, the ferrite powder underwent a two-hour sintering process at a temperature of 950°C. This process resulted in the formation of [$BaFe_{12-2x}Li_xZn_xO_{19}$] ferrite nanoparticles, where x varies as 0.2, 0.4, 0.6, and 0.8, as illustrated in Figure 3 as in Table 1.

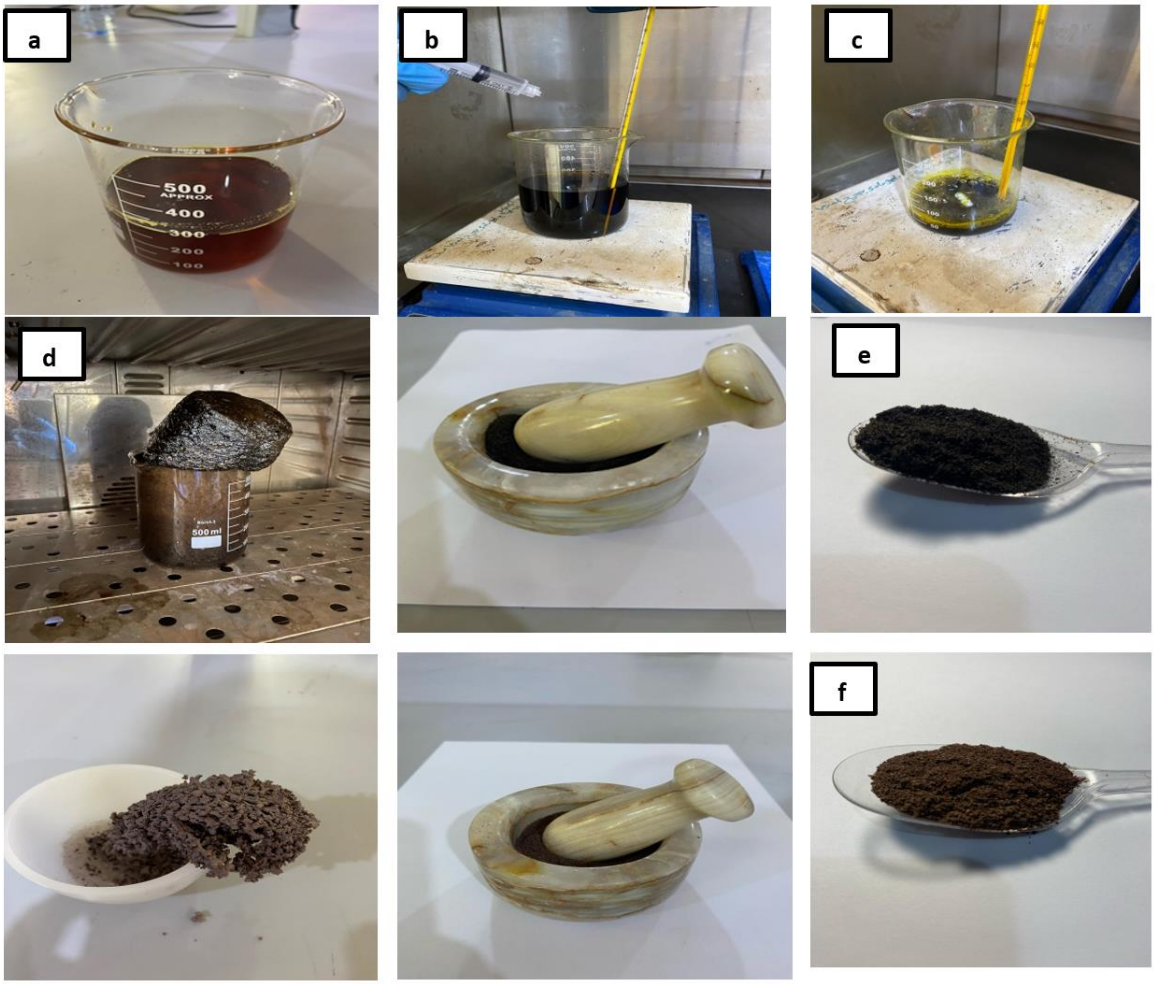

Figure 3.
Phograph of (a) NCS, (b) by additing of ammonia, (c) visc.gel, (d) dry bulk temp.of 200 °C, and (f) AC resulting in nano-powder ferrite.

Table 1.
Details of the symbols used.

Sample name	Material	Sintering temperature
B1	$BaFe_{11.6}Li_{0.2}Zn_{0.2}O_{19}$	950°C
B2	$BaFe_{11.2}Li_{0.4}Zn_{0.4}O_{19}$	950°C
B3	$BaFe_{10.8}Li_{0.6}Zn_{0.6}O_{19}$	950°C
B3	$BaFe_{10.4}Li_{0.8}Zn_{0.8}O_{19}$	950°C

6. Results And Discussion

6.1. XRD diffraction of [$BaFe_{12-2x}Li_xZn_xO_{19}$] ferrite, where (x = 0.2, 0.4, 0.6, and 0.8).

The X-ray diffraction (XRD) pattern matches ICCD card number (00-007-276), and there are no signs of impurities. This shows that the barium hexaferrite we made is pure. This observation shows that

Edelweiss Applied Science and Technology
ISSN: 2576-8484
Vol. 9, No. 2: 2042-2063, 2025
DOI: 10.55214/25768484.v9i2.5043

Zn^{2+} and Li^{1+} ions have been added to the crystal structure without harming it. have been successfully incorporated into the Figure 4b shows that the 114 diffraction peak moves to lower Bragg angles (2θ). This change is due to the difference in size between the ions being replaced, Zn^{2+} (0.74 Å) and Li^{1+} (0.76 Å), and the original ion, Fe^{3+} (0.67 Å).BaFe1. This shift can ionic radii between the substituent Zn^{2+} (0.74 Å) and Li^{1+} (0.76 Å) and the host ion Fe^{3+} (0.67 Å) Li^{1+} ions are larger than Fe^{3+} ions, so when Li^{1+} ions are added, they cause the crystal structure to expand, resulting in larger lattice measurements. Consequently, the unit cell undergoes internal strain, reducing the interplanar spacing (d-spacing) and causing the diffraction peaks to shift systematically to lower angles. This behavior aligns with Bragg's law, which describes the inverse relationship between lattice spacing and diffraction angle. As the substitution level goes up, the diffraction peaks shift to lower 2θ values, showing that the structure of the hexaferrite is changing.

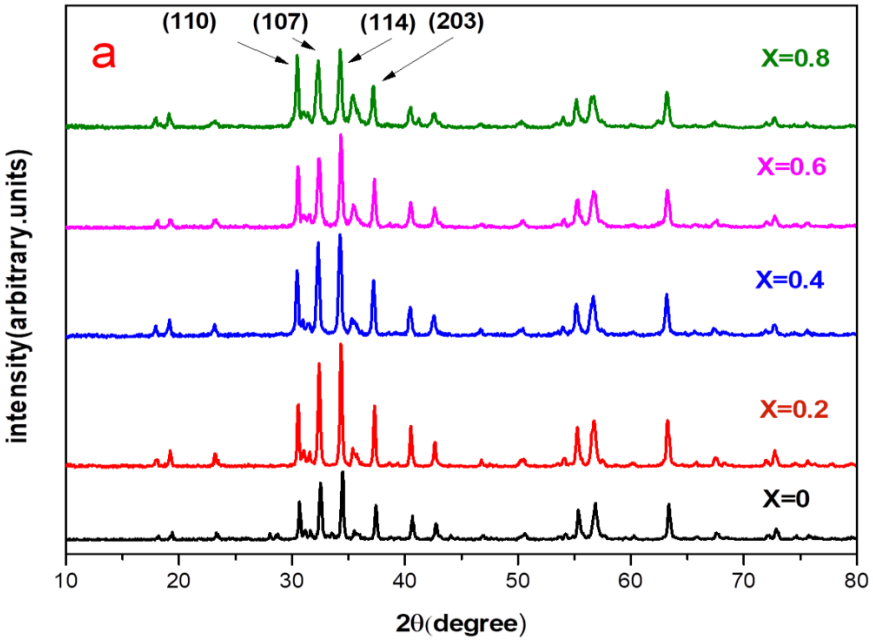

Figure 4a.
Presents the X-ray diffraction (XRD) patterns of Barium Hexaferrite ($BaFe_{12-2x}Li_xZn_xO_{19}$) for varying substitution levels (x = 0.0, 0.2, 0.4, 0.6, and 0.8). The diffraction peaks illustrate the crystallographic structure of the synthesized samples, highlighting the impact of Li-Zn substitution on phase formation and lattice parameters.

Edelweiss Applied Science and Technology
ISSN: 2576-8484
Vol. 9, No. 2: 2042-2063, 2025
DOI: 10.55214/25768484.v9i2.5043

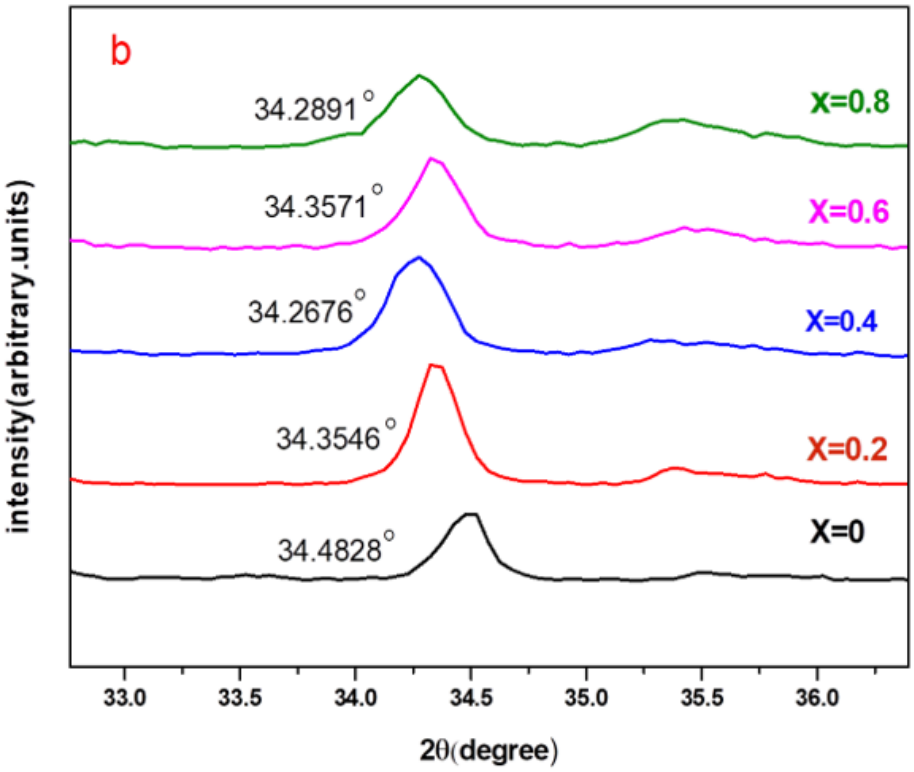

Figure 4b.
Shifts in XRD patterns of (114) XRD peaks due to Zn and Li substitution compared to the pure sample.

$$D = \frac{K\lambda}{\beta \cos\theta} \qquad (1)$$

The results showed in Table 2 As the ionic diameter of both zinc and lithium is larger than the ionic diameter of iron. It was found that the crystal size changes nonlinearly with increasing concentrations of each. This happens because increasing concentration leads to greater lattice stress due to a mismatch of the ionic diameter of zinc and lithium with the ionic diameter of iron. Consequently, crystal growth is impeded under the same preparation conditions Chandra Sekhar, et al. [7].

Table 2.
XRD calculations of [Ba Fe_{12-2x} $Li_xZn_xO_{19}$] sintered at temperature 950°C.

Sample	X	d_{hkl}(°A)	2θ(deg) Standard	FWHM (deg)	Crystalline size(nm)	d_{hkl}(°A) Practical	d_{hkl}(°A) Standard	(hkl)
B1	0.2	34.3546	34.196	0.2460	33.7883	2.6104	2.61898	(114)
B2	0.4	34.2676		0.2952	28.1503	2.6168		
B3	0.6	34.3571		0.2460	33.7886	2.6102		
B4	0.8	34.2891		0.2460	33.7824	2.6152		

The structural properties of these nanoparticles have been determined through precise calculations. These parameters play a crucial role in understanding the crystallographic structure and material behavior. The calculations were performed using the following equations, which are fundamental in analyzing the geometric and physical characteristics of the unit cell [8]:

$$\frac{1}{d_{hkl}^2} = \frac{4}{3}\left(\frac{h^2+hk+k^2}{a^2}\right) + \frac{l^2}{c^2} \quad (2)$$

$$V = 0.8666a^2c \quad (3)$$

Edelweiss Applied Science and Technology
ISSN: 2576-8484
Vol. 9, No. 2: 2042-2063, 2025
DOI: 10.55214/25768484.v9i2.5043

Table 3 presents the lattice parameters, unit cell volume (V_cell), and crystal axis contraction ratio (c/a) of substituted hexaferrite nanoparticles. The data show a nonlinear variation in these parameters with increasing substitution, with the c-axis exhibiting more significant changes than the a-axis, particularly when Zn and Li ions are introduced.: a = b = 5.8650 – 5.8820 °A and c = 23.088 – 23.170 °A, with an increase in the variable 'x. Consequently, the unit cell volume (V_{cell}) change from 692.11 to 708.34 $Å^3$. with maximum values observed at x = 0.4.this change is attributed to the internal stress that causes the lattice to deform and leads to large expansion of the unit cell at this concentration[7]. It is know that if the value of c/a (crystal axis contraction ratio) is less than 3.98, the structure is considered to be a hexagonal structure of type M [8].

Table 3.
MSet. characteristics of [$BaFe_{12-2x}Li_xZn_xO_{19}$] other contents(x=0.2, 0.4, 0.6 and 0.8).

Sample	x	d_{hkl}(°A)	Lattice Constant a=b (°A)	Lattice Constant c (°A)	c/a	V(°A)^3
-	0.0	2.9097	5.8195	23.077	3.965	676.83
B1	0.2	2.6104	5.8650	23.088	3.936	688.24
B2	0.4	2.6168	5.8780	23.170	3.941	693.75
B3	0.6	2.6102	5.8650	23.088	3.938	688.24
B4	0.8	2.6152	5.8820	23.099	3.927	691.34

6.2. Energy Dispersive Spectroscopy (EDS) of [$BaFe_{12-2x}Li_xZn_xO_{19}$] Ferrite, Where (x = 0.2, 0.4, 0.6, and 0.8).

This technique provides a quantitative analysis of elemental composition by detecting the characteristic X-ray emissions from the sample. The results validate the successful incorporation of substituent ions into the $BaFe_{12-2x}Li_xZn_xO_{19}$ lattice without any significant deviations from the intended stoichiometry, ensuring the structural integrity and phase purity of the synthesized material., elemental analysis was conducted using energy-dispersive spectroscopy (EDS). This technique will provide a detailed assessment of the. elemental distribution within the synthesized material. The obtained results, presented the table within the figure, confirm the successful incorporation of\the intended elements. indicating the reliability of the synthesis process and the effective substitution of Li and Zn ions within the crystal structure. Figure (5) shows the EDS spectra of samples with B1, B2, B3, and B4, where peaks of Ba, Fe, Zn, and O elements can be observed; however, this spectrum does not include any peak for the element lithium due to its low characteristic energy radiation and its low concentration in the prepared samples [9, 10]. The EDS study indicates that as the concentration of substituted ions increased from x = 0.2 to x = 0.8, the weight percentage of iron decreased from 57.3050% to 52.8825%, while the weight percentage of zinc increased from 0.605% to 3.0125%, respectively.

The proportions of the compositional elements measured align with those predicted by the stoichiometric formula. Additionally, the EDS spectra reveal that the intensity of the zinc peaks increased, while the intensity of the iron peaks decreased with increasing values of (x), indicating that substituted ions incorporate well into the ferrite structure. Importantly, the spectra confirm that the samples produced do not contain trace amounts of any contaminants or impurities [11].

Edelweiss Applied Science and Technology
ISSN: 2576-8484
Vol. 9, No. 2: 2042-2063, 2025
DOI: 10.55214/25768484.v9i2.5043

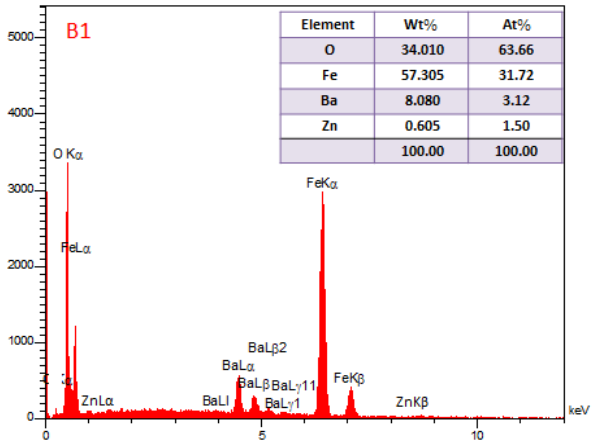

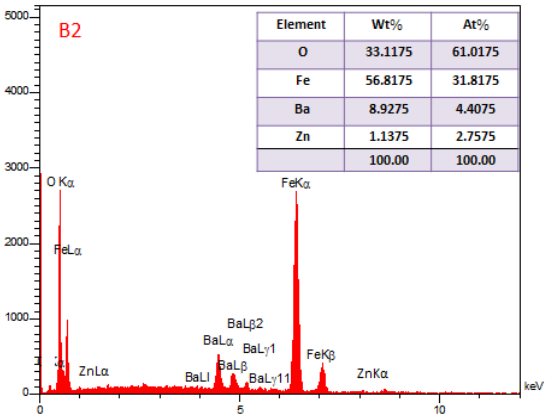

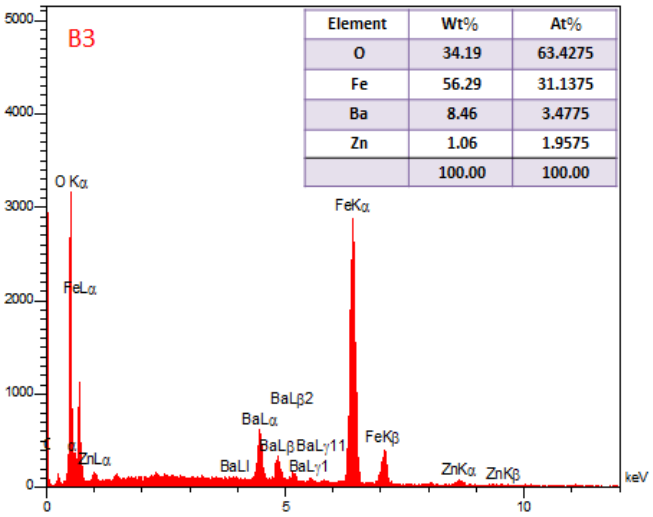

Edelweiss Applied Science and Technology
ISSN: 2576-8484
Vol. 9, No. 2: 2042-2063, 2025
DOI: 10.55214/25768484.v9i2.5043

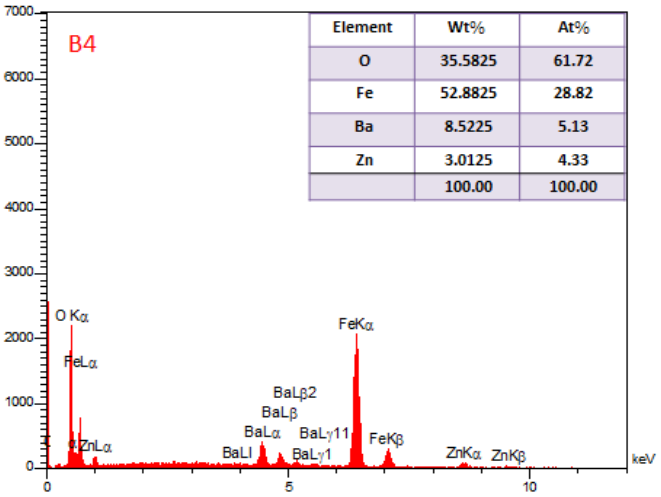

Figure 5.
The typical EDS spectra of substituted hexaferrite nanoparticles: B1 (X=0.2), B2 (X=0.4), B3 (X=0.6), B4 (X=0.8).

7. Morphological Characterization

The morphology of the substituted hexaferrite nanoparticles was analyzed using Field Emission Scanning Electron Microscopy (FE-SEM), with the resulting micrographs presented in Fig. 5. The rectangular hexagonal structure is evident in all samples, and the nanoparticles exhibit homogeneity and a closely packed arrangement across the surface. The mean particle diameters for BaFe12−2xLixZnxO19 (with x values of 0.2, 0.4, 0.6, and 0.8) in samples B1, B2, B3, and B4 are 74.09 nm, 70.46 nm, 53.45 nm, and 56.10 nm, respectively. The ion substitution in the hexagonal structure of barium ferrite leads to a decrease in particle size relative to pure barium ferrite. This reduction can be attributed to suppressed growth on specific crystallographic planes, while facilitating growth in alternative directions. The presence of substituted ions at grain boundaries can impede grain growth. The inclusion of substituted elements with larger ionic radii than Fe3+, coupled with internal stress, impedes grain growth [12]. Figure 6 demonstrates that an increase in x content results in the elongation of grains, which adopt an elongated plate or rod-like morphology. The trend toward rod-like morphology significantly affects the magnetic properties of the samples, which will be addressed subsequently. The average particle size obtained from SEM measurements exceeds the average crystallite size measured by X-ray Diffraction (XRD), suggesting that each particle consists of multiple aggregated crystallites [13].

Edelweiss Applied Science and Technology
ISSN: 2576-8484
Vol. 9, No. 2: 2042-2063, 2025
DOI: 10.55214/25768484.v9i2.5043

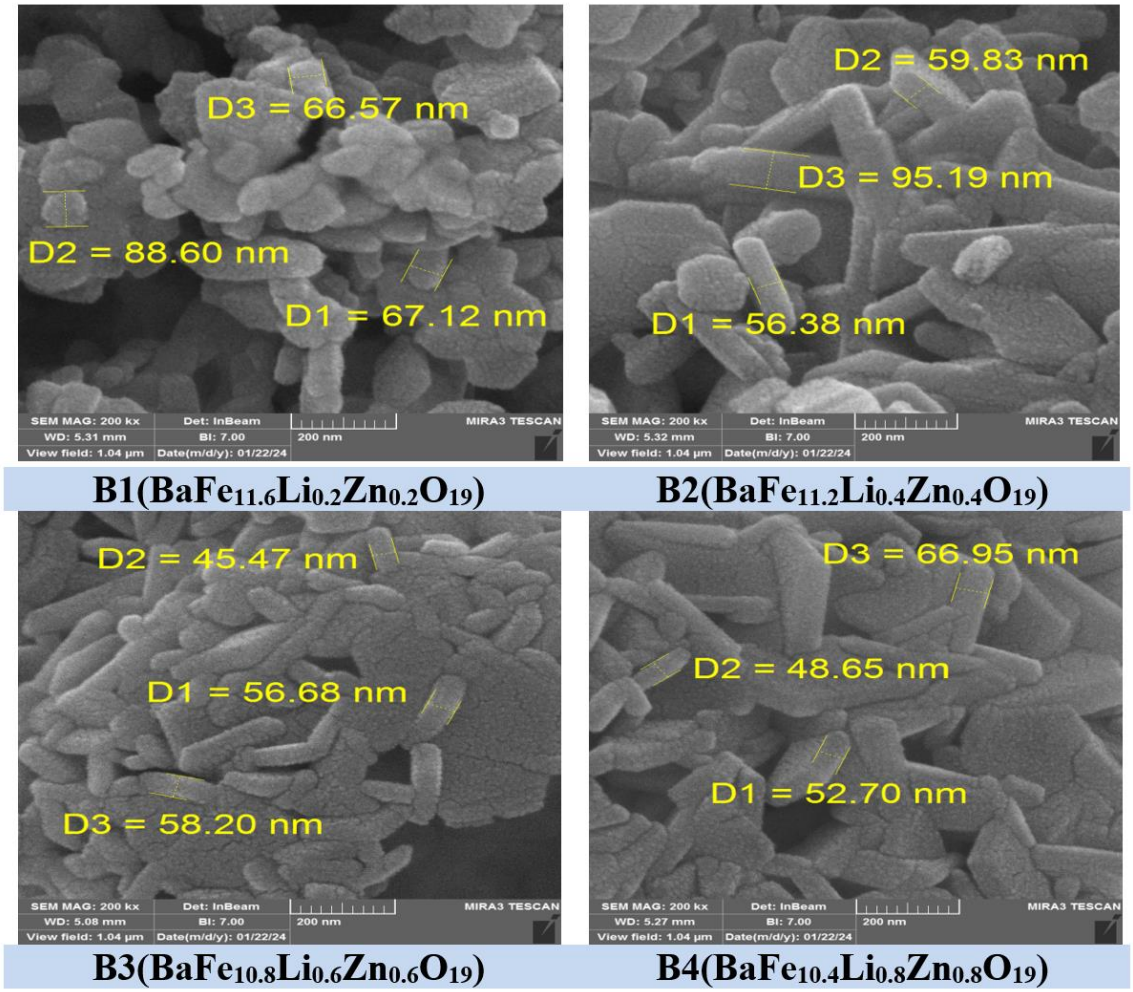

Figure 6.
FE-SEM images of $BaFe_{12-2x}Li_xZn_xO_{19}$ hexagonal ferrite nanoparticles for the values of (x = 0.2, 0.4, 0.6, and 0.8).

8. Magnetic Characterization

8.1.Vibrating Sample Magnetometer (VSM) analysis of ($BaFe_{12-2x}Li_xZn_xO_{19}$) nanoparticles with varying compositions (x = 0.2, 0.4, 0.6, and 0.8) was conducted at a sintering temperature of 950°C for 2 hours.

Figure 7 shows hysteresis loopsof (M–H curves)The findings demonstrate that an increase in the quantity of substituted ions within the composition correlates with an enhancement in saturation magnetization. (Ms) and remanent magnetization (Mr) decrease, reaching minimum values of 5.462 emu/g and 7.08 emu/g, respectively. In contrast, the coercive field (Hc) increases, particularly at x = 0.4, where it reaches a maximum value of 4358 Oe, and then decreases with increasing substitution ions. Additionally, the shape of the grains affects coercivity as well, due to the significant impact of grain shape on the anisotropy of the crystals. It is assumed that the Hc value adheres to the following proportion:

$$Hc \propto \frac{K}{M_s} \qquad (8)$$

Here, K denotes the magnetocrystalline anisotropy constant. From Equation (8), we can conclude that coercivity (Hc) is directly proportional to the anisotropy constant (K) and inversely proportional to the saturation magnetization (Ms). By analyzing the variations in K and Ms that occur as the grain size decreases, we can also determine how Hc changes. Initially, we will focus on the alterations in K. As

Edelweiss Applied Science and Technology
ISSN: 2576-8484
Vol. 9, No. 2: 2042-2063, 2025
DOI: 10.55214/25768484.v9i2.5043

previously mentioned, scanning electron microscopy (SEM) images confirm that with an increase in the number of substituted ions, the grains, which initially exhibit a hexagonal plate-like structure, tend to transform into a rod-like shape. This morphological change results in decreased crystal symmetry, leading to an increase in the anisotropy constant (K) and, consequently, an increase in magnetic coercivity (Hc). Furthermore, the squareness ratio (Mr/Ms) exceeds the theoretical value of 0.5, indicating that the hexaferrite powders possess strong uniaxial anisotropy. Nanomaterials form the basis of major areas of science and technology; hence, the knowledge of additional facts, including their preparation and characterization, will enhance the development of suitable methods to yield high-quality nanomaterials. In this case, the magnetic nano powder Li0.35Zn0.10Ba0.10Fe2.45O4 (LZBF). The XRD results of this LZBF nano powder depict the indexed Miller's indices values of simultaneously existing planes h, k, and l to the cubic spinel structure of the LZBF nano powder. The implication of this result falls within the final result, which is immensely capable for bio-application; specifically, hyperthermia and drug delivery. In this work, new perspectives to conduct LZBF applications were implemented in order to reinvent innovative methods against cancer.

However, in future studies, enhanced detailed investigation through industries and corporate dimensions is required to unravel the enormous potential and to provide optimum applications that could trigger modernized protocols of drug delivery systems and the so-called magnetic hyperthermia. In this regard, extensive research should be engaged at the interdisciplinary dimension in basic medical and bioscience, especially relating to Molecular Medicine, Pharmacognosy, Biochemistry, and Nanosciences in developing modern clinical applications. Additionally, in the future, modified physico-chemical techniques are to be explored by involving additional instrumentation techniques in the course of synthesis and preparation of LZBF to guarantee optimum results and their modern derivatives. With these strategies in consonance, the result will undoubtedly break up current therapeutic management pathways in order to allow advances that will be of best suitable interest to mankind.

Table 4.
(Ms), (Hc), (Mr), (Mr/Ms) $[BaFe_{12-2x}Li_xZn_xO_{19}]$ nanoparticles for various compositions (x = 0.2, 0.4, 0.6, and 0.8).

Sample	X	Ms (emu/g)	Hc (Oe)	Mr (emu/g)	Mr/Ms
B1	0.2	13.197	1166	8.200	0.62
B2	0.4	7.087	4358	5.462	0.77
B3	0.6	12.447	4070	7.446	0.59
B4	0.8	12.016	3053	6.656	0.55

Edelweiss Applied Science and Technology
ISSN: 2576-8484
Vol. 9, No. 2: 2042-2063, 2025
DOI: 10.55214/25768484.v9i2.5043

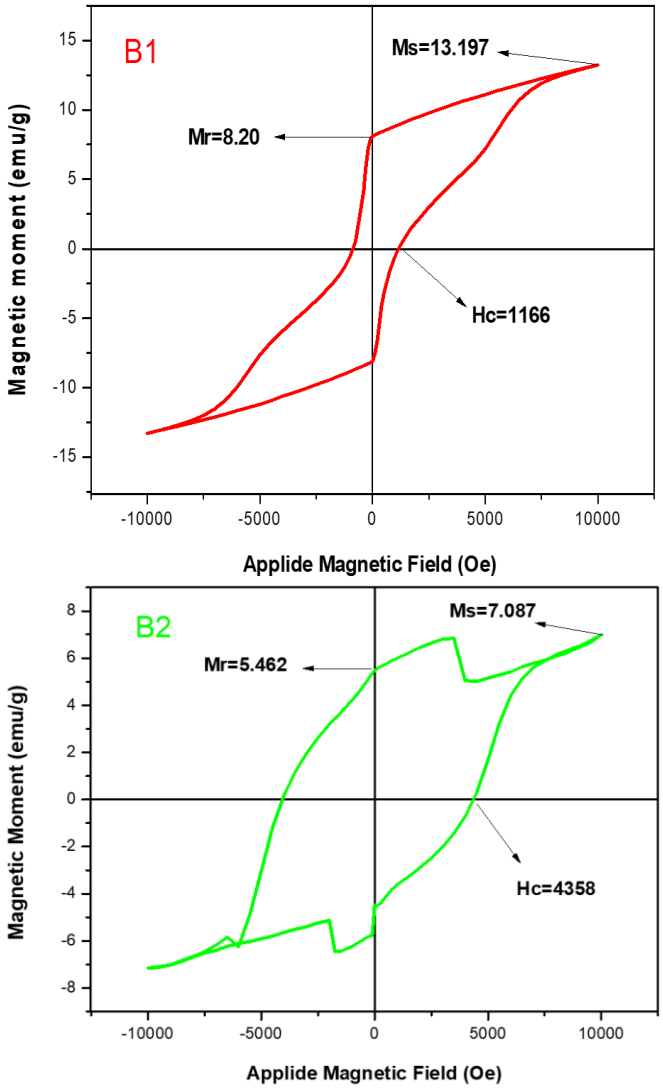

Edelweiss Applied Science and Technology
ISSN: 2576-8484
Vol. 9, No. 2: 2042-2063, 2025
DOI: 10.55214/25768484.v9i2.5043

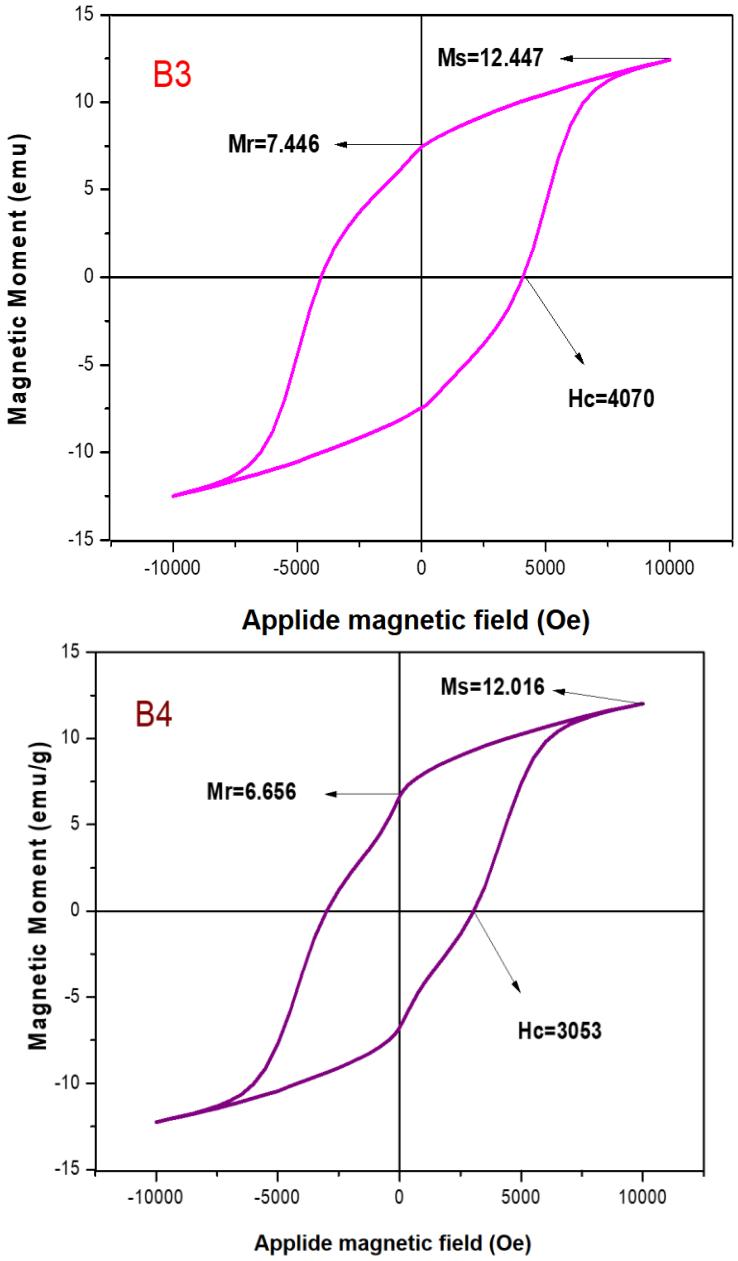

Figure 7.
TH loops of barium ferrite nanoparticles, specifically the $BaFe_{12-2X}Li_xZn_xO_{19}$ series, where B1 corresponds to x = 0.2, B2 to x = 0.4, B3 to x = 0.6, and B4 to x = 0.8.

9. Anti.Ba. Activity

The effectiveness of the made samples (B1, B2, B3, and B4) against two types of bacteria—Gram-positive (Staphylococcus aureus) and Gram-negative (Proteus mirabilis)—was tested using the agar well diffusion method. This technique is commonly employed to assess the antimicrobial properties of materials through the measurement of inhibition zones surrounding the tested samples.

Edelweiss Applied Science and Technology
ISSN: 2576-8484
Vol. 9, No. 2: 2042-2063, 2025
DOI: 10.55214/25768484.v9i2.5043

The bacterial cultures were uniformly applied to the agar surface to establish a consistent lawn of microbial growth.

Next, 6 mm wells were made in the agar using a clean tool, which kept the well sizes the same for accurate comparisons. Different concentrations :of the test samples (B1, B2, B3, and B4) were systematically added to these wells. The bacteria and test samples were kept at 37°C for 24 hours to allow enough bacteria to grow and interact with the Anti.Ba. agents.

. our results, demonstrating Anti.Ba. performance across various sampl concentrations are presented in the figures.

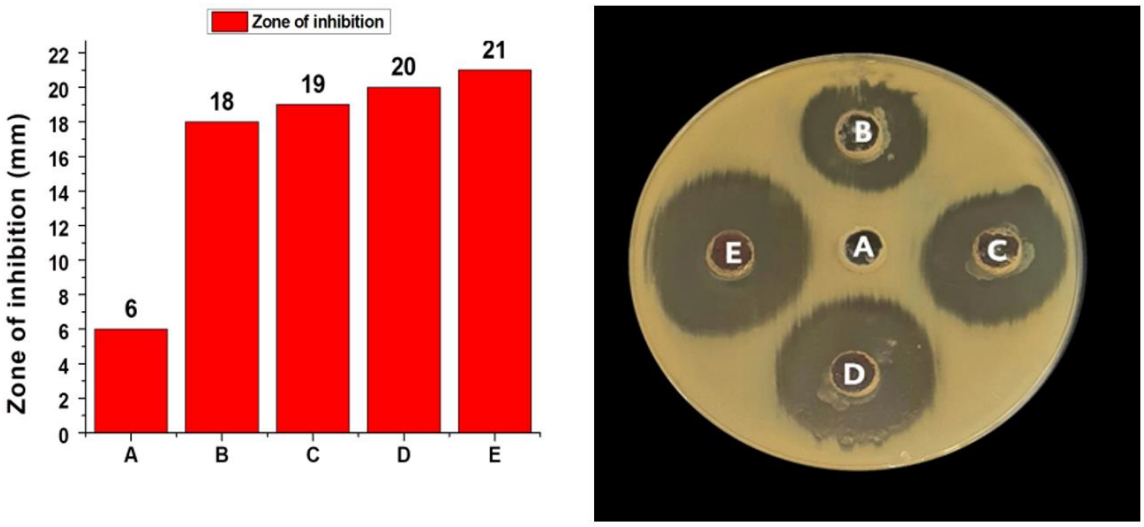

Figure 8.
Anti-Ba activity of (B1) against S. aureus. A control. B has a concentration.

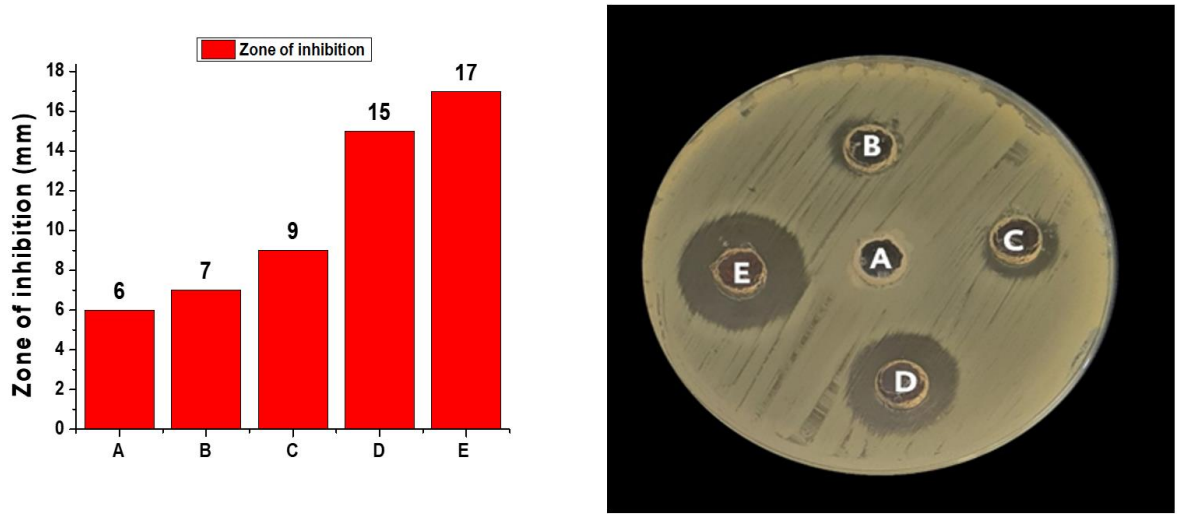

Figure 9.
Anti-Ba activity of (B1) against Proteus mirabilis. A: Control. B is measured.

Edelweiss Applied Science and Technology
ISSN: 2576-8484
Vol. 9, No. 2: 2042-2063, 2025
DOI: 10.55214/25768484.v9i2.5043

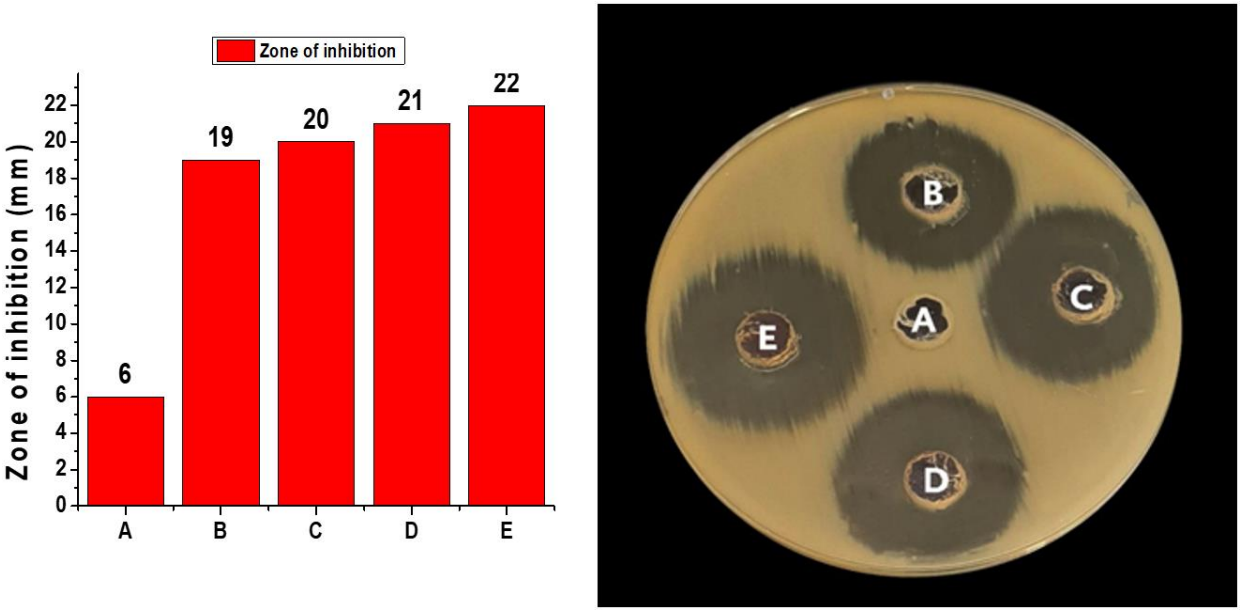

Figure 10.
Anti-Ba activity of (B2) against S. aureus. A: Control. B has a concentration of 31.2 µg/ml. C concentration is 62.5 µg/ml.

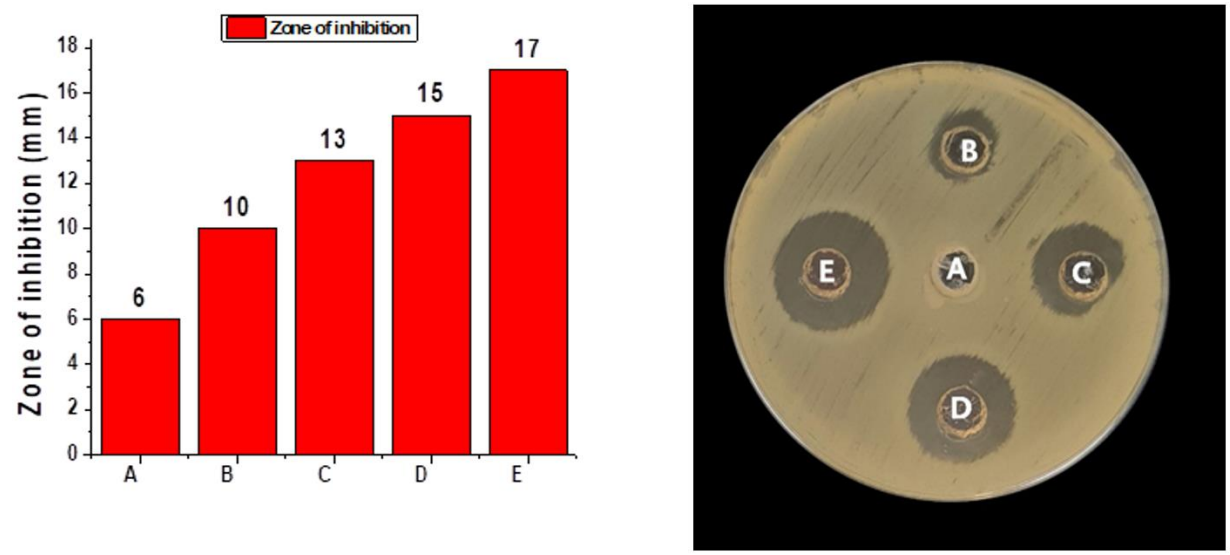

Figure 11.
Antibacterial activity of (B2) against Proteus mirabilis. A, Regulation. Substance B has a concentration of 31.2 µg/ml. C, 62.5 micrograms per milliliter. D at a concentration of 125 micrograms per milliliter. E at a concentration of 250 micrograms per milliliter.

Edelweiss Applied Science and Technology
ISSN: 2576-8484
Vol. 9, No. 2: 2042-2063, 2025
DOI: 10.55214/25768484.v9i2.5043

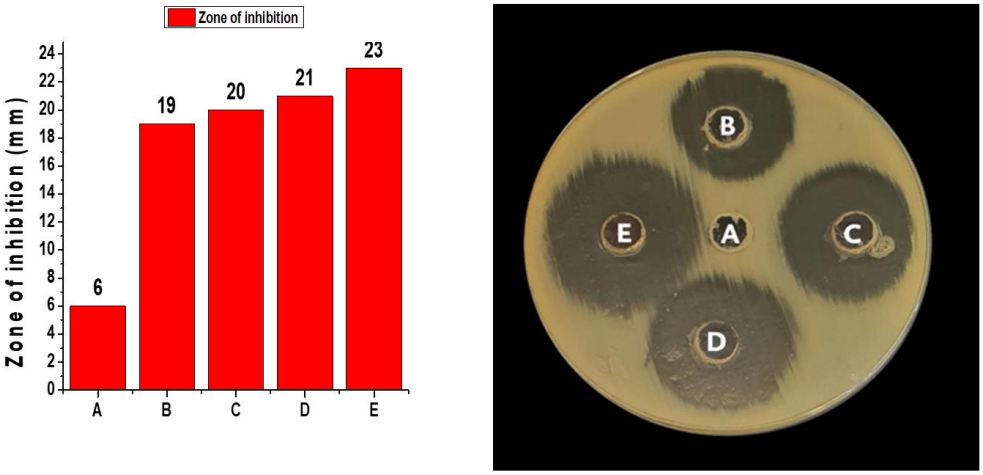

Figure 12.
Antibacterial activity of (B3) against Staphylococcus aureus. A, Regulation. B is quantified at 31.2 µg/ml. C, 62.5 micrograms per milliliter. D at a concentration of 125 micrograms per milliliter. E at a concentration of 250 micrograms per milliliter.

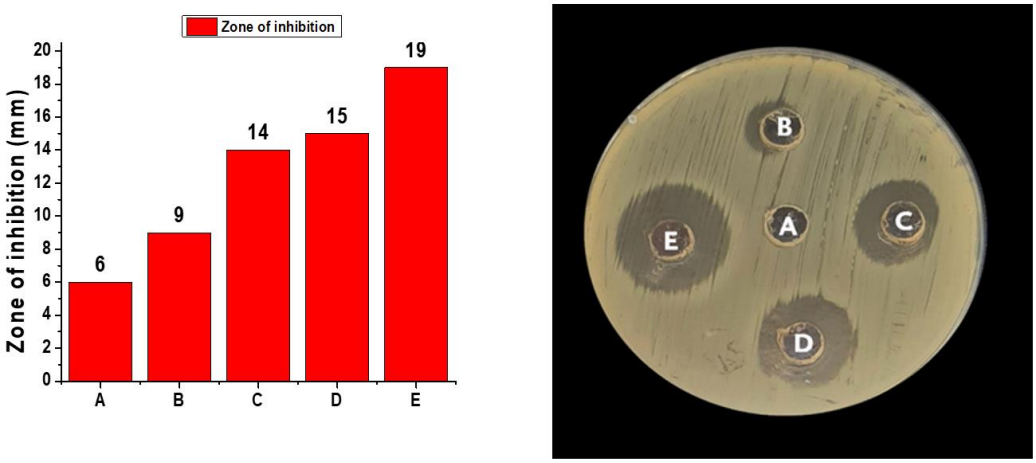

Figure 13.
Antibacterial activity of (B3) against Proteus mirabilis. A, Regulation. B, 31.2 micrograms per milliliter. C, 62.5 micrograms per milliliter. D at a concentration of 125 µg/ml. E concentration.

Edelweiss Applied Science and Technology
ISSN: 2576-8484
Vol. 9, No. 2: 2042-2063, 2025
DOI: 10.55214/25768484.v9i2.5043

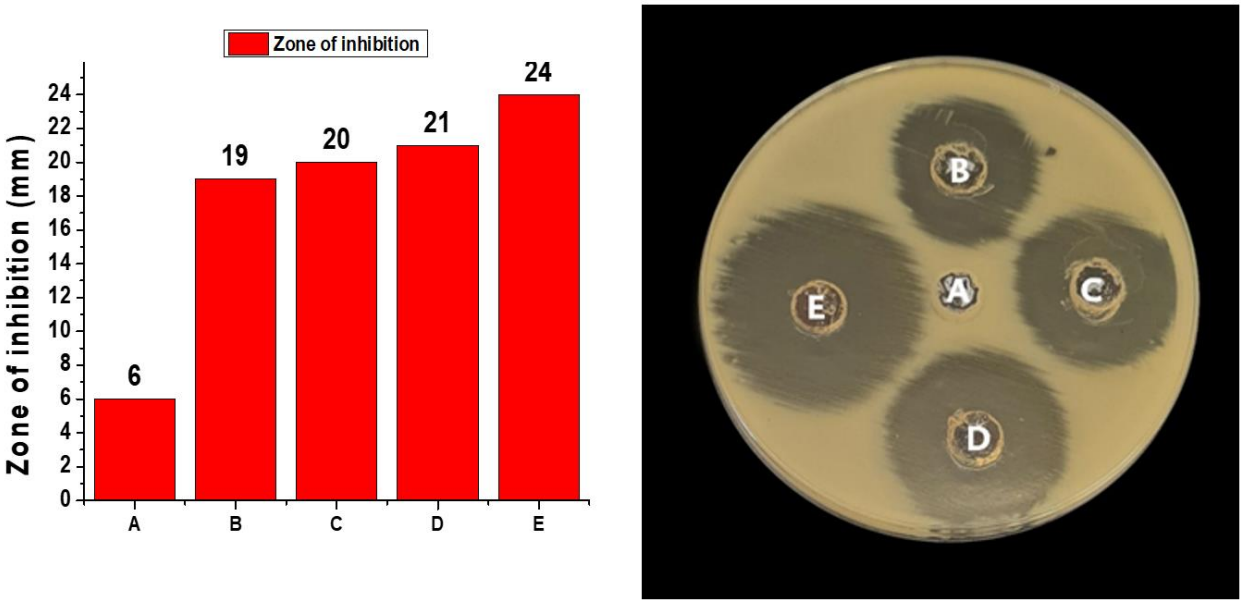

Figure 14.
Antibacterial activity of (B4) against Staphylococcus aureus. A: Control; B: 31.2 µg/ml. C, 62.5 micrograms per milliliter. D, 125 micrograms per milliliter. E at a concentration of 250 µg/ml.

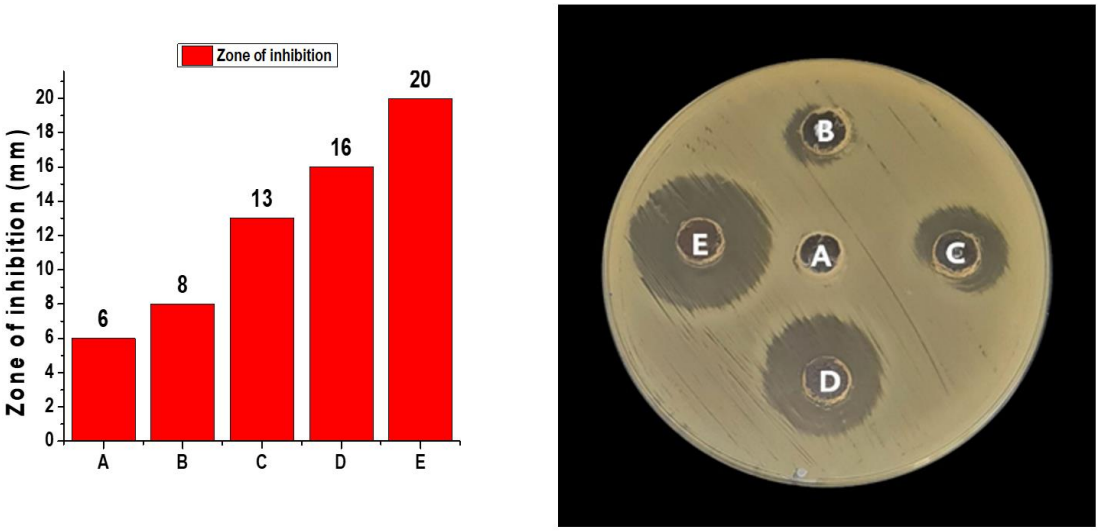

Figure 15.
Antibacterial activity of (B4) against Proteus mirabilis. A, Regulation. B, 31.2 micrograms per millliliter. C, 62.5 micrograms per milliliter. D at a concentration of 125 µg/ml. E at a concentration of 250 µg/ml.

In experiments conducted at the highest concentration (250µg/ml), the inhibition zones formed by barium ferrites substituted were found to be larger for Staphylococcus aureus compared to Proteus mirabilis. Specifically, an inhibition zone measuring 24 mm was observed for Staphylococcus aureus, while for Proteus mirabilis, the zone measured 20 mm. (Ba2+, Zn2+, and Fe3+) in killing bacteria that penetrate the bacterial wall and has a toxic nature, this process can lead to a loss of membrane flexibility. Additionally, nanoparticles are capable of penetrating bacterial cell walls, which alters membrane permeability. Such disruption makes it challenging for the cell to regulate the entry of substances through the cytoplasmic membrane, ultimately contributing to cell death. Furthermore, nanoparticles interfere

Edelweiss Applied Science and Technology
ISSN: 2576-8484
Vol. 9, No. 2: 2042-2063, 2025
DOI: 10.55214/25768484.v9i2.5043

with transcription and can cause DNA damage, accelerating mutagenesis. They also negatively impact mitochondria and disrupt their metabolism, leading to an imbalance in cellular energy levels. Moreover, nanoparticles hinder the formation of lysosomes, impairing autophagy and the degradation of macromolecules, which can trigger apoptosis. Additionally, nanoparticles stimulate the production of inflammatory mediators by disrupting normal cellular, tissue, and organ metabolism [14]. They also inhibit the formation of biofilms, which are protective layers of lipopolysaccharides (1–3 μm thick) encasing bacterial cells. These biofilms serve as barriers that shield cells from the immune system and enhance their resistance to antibiotics [15]. Due to their magnetic and Anti.Ba. properties, nanoparticles prepared using the sol-gel method can be utilized in drug delivery systems [16].

10. Conclusion

Nanosized barium ferrites, specifically $BaFe_{12-2x}Li_xZn_xO_{19}$ (where x = 0.2, 0.4, 0.6, and 0.8), were successfully synthesized using an auto-combustion sol-gel process with substitutions of Zn^{2+} and Li^{+}. X-ray diffraction (XRD) analysis confirmed that all synthesized compounds exhibited a single-phase M-type hexagonal structure. Scanning electron microscopy (SEM) analysis showed that as the content of x increased, the grains tended to elongate, taking on an elongated plate or rod-like shape. Energy dispersive spectroscopy (EDS) spectra indicated that the intensity of the zinc peaks increased while the intensity of the iron peaks decreased with higher values of x, indicating that substituted ions incorporate well into the ferrite structure. Importantly, these spectra confirmed that the produced samples contained no trace amounts of contaminants or impurities. Fourier-transform infrared (FTIR) analysis revealed bond, while the peaks between 540–584 cm^{-1} corresponded to the stretching vibrations of the metal-oxygen bond (Ba-O). Regarding magnetic properties (Ms, Mr, and Hc), the results indicated that both saturation magnetization (Ms) and remanent magnetization (Mr) decreased as the amount of substituted ions increased, reaching minimum values of 5.462 emu/g and 7.08 emu/g, respectively. In contrast, the coercive field (Hc) increased, particularly at x = 0.4, where it reached a maximum value of 4358 Oe before decreasing with further increases in substitution ions. Additionally, the Anti.Ba. potential of the prepared samples was examined. It was found that Staphylococcus aureus bacteria demonstrated greater sensitivity than Proteus mirabilis in agar diffusion tests. This increased sensitivity is attributed to the greater resistance of Gram-negative bacteria, which possess an additional lipid membrane that hinders the passage of nanoparticles.

Transparency:

The authors confirm that the manuscript is an honest, accurate, and transparent account of the study; that no vital features of the study have been omitted; and that any discrepancies from the study as planned have been explained. This study followed all ethical practices during writing.

References

[1] N. Ibrahim, Y. Noratiqah, M. Jailani, and E. Iruthayaraj, "Improved structural and magnetic properties of a non-stoichiometry Ba: Fe ratio of barium hexaferrite film," *Applied Physics A*, vol. 126, pp. 1-8, 2020. https://doi.org/10.1007/s00339-020-03497-w

[2] I. Auwal, A. Baykal, H. Güngüneş, and S. E. Shirsath, "Structural investigation and hyperfine interactions of BaBixLaxFe12− 2xO19 (0.0≤ x≤ 0.5) hexaferrites," *Ceramics International*, vol. 42, no. 2, pp. 3380-3387, 2016. https://doi.org/10.1016/j.ceramint.2015.10.095

[3] H. Sözeri, Z. Mehmedi, H. Kavas, and A. Baykal, "Magnetic and microwave properties of BaFe12O19 substituted with magnetic, non-magnetic and dielectric ions," *Ceramics International*, vol. 41, no. 8, pp. 9602-9609, 2015. https://doi.org/10.1016/j.ceramint.2015.04.138

Edelweiss Applied Science and Technology
ISSN: 2576-8484
Vol. 9, No. 2: 2042-2063, 2025
DOI: 10.55214/25768484.v9i2.5043

[4] P. P. Mohapatra and P. Dobbidi, "Magnetic, optical, and impedance spectroscopy of barium-substituted lithium ferrite," *The Journal of Physical Chemistry C*, vol. 125, no. 25, pp. 14014-14026, 2021. https://doi.org/10.1021/acs.jpcc.1c03149

[5] M. K. Manglam, S. Kumari, L. K. Pradhan, S. Kumar, and M. Kar, "Lattice strain caused magnetism and magnetocrystalline anisotropy in Zn modified barium hexaferrite," *Physica B: Condensed Matter*, vol. 588, p. 412200, 2020. https://doi.org/10.1016/j.physb.2020.412200

[6] Z. M. A. Abbas, W. A. Shatti, M. M. Kareem, and Z. T. Khodair, "Synthesis and characterization of NiFe2O4/CuO nanocomposites: Structural and magnetic properties analysis," *Chemical Data Collections*, vol. 47, p. 101078, 2023. https://doi.org/10.1016/j.chemdat.2023.101078

[7] D. Chandra Sekhar, T. Subba Rao, and K. Chandra Babu Naidu, "Iron deficient BaNi x Mn x Fe12− 2 x O19 (x= 0.0–0.5) hexagonal plates: Single-domain magnetic structure and dielectric properties," *Applied Physics A*, vol. 126, no. 7, p. 511, 2020. https://doi.org/10.1007/s00339-020-35257-7

[8] R. El Shater, E. El-Ghazzawy, and M. El-Nimr, "Study of the sintering temperature and the sintering time period effects on the structural and magnetic properties of M-type hexaferrite BaFe12O19," *Journal of Alloys and Compounds*, vol. 739, pp. 327-334, 2018. https://doi.org/10.1016/j.jallcom.2017.12.115

[9] T. S. Santoshi, S. Bharadwaj, M. C. Varma, V. Dhand, and G. Choudary, "Structural and magnetic properties of α-Fe2O3 with lithium ferrite prepared using co-precipitation method and annealed at different temperatures," *Chemical Physics Impact*, vol. 9, p. 100717, 2024. https://doi.org/10.1016/j.cphip.2024.100717

[10] S. Muto and K. Tatsumi, "Detection of local chemical states of lithium and their spatial mapping by scanning transmission electron microscopy, electron energy-loss spectroscopy and hyperspectral image analysis," *Microscopy*, vol. 66, no. 1, pp. 39-49, 2017. https://doi.org/10.1093/jmicro/dfw050

[11] A. G. Awni and Z. M. A. Abbas, "Morphological and structural properties of bismuth-nickel ferrite synthesized by a combined sol-gel method," *Nexo Revista Científica*, vol. 36, no. 06, pp. 1076-1086, 2023.

[12] N. Yasmin *et al.*, "Impact of Ho-Ni substitution on structural, morphological and dielectrical characteristics of BaFe12O19 M-type hexagonal ferrite," *Physica B: Condensed Matter*, vol. 581, p. 411950, 2020. https://doi.org/10.1016/j.physb.2019.411950

[13] A. Shayan, M. Abdellahi, F. Shahmohammadian, S. Jabbarzare, A. Khandan, and H. Ghayour, "Mechanochemically aided sintering process for the synthesis of barium ferrite: Effect of aluminum substitution on microstructure, magnetic properties and microwave absorption," *Journal of Alloys and Compounds*, vol. 708, pp. 538-546, 2017. https://doi.org/10.1016/j.jallcom.2017.02.022

[14] A. Sukhanova, S. Bozrova, P. Sokolov, M. Berestovoy, A. Karaulov, and I. Nabiev, "Dependence of nanoparticle toxicity on their physical and chemical properties," *Nanoscale Research Letters*, vol. 13, pp. 1-21, 2018. https://doi.org/10.1186/s11671-018-2655-7

[15] Y. N. Slavin, J. Asnis, U. O. Hńfeli, and H. Bach, "Metal nanoparticles: Understanding the mechanisms behind antibacterial activity," *Journal of Nanobiotechnology*, vol. 15, pp. 1-20, 2017. https://doi.org/10.1186/s12951-017-0308-0

[16] S. C. Watawe, V. Mujumdar, and R. S. Chaughule, "Nanotechnology in drug administration and food," *Journal of Nanoscience and Nanotechnology*, vol. 9, no. 11, pp. 6345-6353, 2009.

Edelweiss Applied Science and Technology
ISSN: 2576-8484
Vol. 9, No. 2: 2042-2063, 2025
DOI: 10.55214/25768484.v9i2.5043